Enhanced ammonium removal and recovery from municipal wastewater by asymmetric CDI cell equipped with oxygen functionalized carbon electrode

Pastushok Olga, Ramasamy Deepika, Sillanpää Mika, Repo Eveliina

DOI: 10.1016/j.seppur.2021.119064

Enhanced ammonium removal and recovery from municipal wastewater by asymmetric CDI cell equipped with oxygen functionalized carbon electrode

Olga Pastushok [a1*], Deepika L. Ramasamy [a1], Mika Sillanpää [bcdefghij], Eveliina Repo [a2]

[a] *Department of Separation Science, School of Engineering Science, Lappeenranta-Lahti University of Technology (LUT),* [1] *Sammonkatu 12, Mikkeli, FI-50130/* [2] *Skinnarilankatu 34, Lappeenranta, FI-53850, Finland*

[b] *School of Civil Engineering and Surveying, Faculty of Health, Engineering and Sciences, University of Southern Queensland, West Street, Toowoomba, 4350 QLD, Australia*

[c] *Department of Chemical Engineering, School of Mining, Metallurgy and Chemical Engineering, University of Johannesburg, P. O. Box 17011, Doornfontein 2028, South Africa*

[d] *School of Civil Engineering and Surveying, Faculty of Health, Engineering and Sciences, University of Southern Queensland, West Street, Toowoomba, 4350 QLD, Australia*

[e] *Department of Chemical Engineering, School of Mining, Metallurgy and Chemical Engineering, University of Johannesburg, P. O. Box 17011, Doornfontein 2028, South Africa*

[f] *School of Chemical and Metallurgical Engineering, University of the Witwatersrand, 2050 Johannesburg, South Africa*

[g] *Chemistry Department, College of Science, King Saud University, Riyadh 11451, Saudi Arabia*

[h] *School of Resources and Environment, University of Electronic Science and Technology of China (UESTC), NO. 2006, Xiyuan Ave., West High-Tech Zone, Chengdu, Sichuan 611731, P.R. China*

[i] *Faculty of Science and Technology, School of Applied Physics, University Kebangsaan Malaysia, 43600, Bangi, Selangor, Malaysia*

[j] *School of Chemistry, Shoolini University, Solan, Himachal Pradesh, 173229, India*

**Corresponding author.*

E-mail address: olga.pastushok@lut.fi (O. Pastushok)

ABSTRACT

Following the concept of sustainable development and circular economy, the Capacitive Deionization (CDI) was examined for the removal and recovery of ammonium (NH_4^+) ions from municipal wastewater towards prevention of eutrophication and obtaining a valuable component for fertilizers production. The electrosorption study was conducted in the symmetric CDI cell, composed of activated carbon (AC) electrodes, and an asymmetric CDI cell, equipped with oxygen functionalized AC (AC-ox) cathode. The asymmetric CDI cell was demonstrated the enhanced performance in terms of the removal efficiency towards ammonium ions (83%) and the related energy consumption (and 0.085 kWh/mmol NH_4^+), compared to the symmetric one with the following results: 30% removal of NH_4^+ ions and 0.215 kWh/mmol NH_4^+. The beneficial performance of the AC-ox electrode also has been observed in terms of NH_4^+ recovery: 20% recovered NH_4^+ ions, compared to 9% NH_4^+ recovered ions by AC pristine electrode. The presence of competitive ions hindered the electrosorption efficiency. Nevertheless, the time-dependent selectivity of the AC-ox electrode towards NH_4^+ ions was observed. The specific capacities of the symmetric and asymmetric cells at 5 mV/s were calculated to be 10.4 F/g and 18.3 F/g, respectively. Material characterization of AC before and after oxidation explained the enhanced CDI performance of the AC-ox electrode due to the increased hydrophilicity and additional oxygen functionalities on the electrode surface.

Keywords: activated carbon electrode**;** oxidation; capacitive deionization; ammonium ions; electrosorption; desorption.

1. Introduction

Rapid population growth is fraught with problems leading to the rise in demand for food production and water pollution [1]. The role of nitrogen is ambiguous for both issues. On the one hand, nitrogen compounds discharged through the wastewater into water bodies cause eutrophication and the deterioration of the water ecosystem [2]. On the other hand, nitrogen compounds are essential for plant growth, usually supplied in the form of ammonium through fertilizers [3]. The annual consumption of nitrogen fertilizers is about 111 MT [4]. Although atmospheric nitrogen is ubiquitous, much energy is consumed to convert nitrogen into ammonia, used for nitrogen fertilizers, by the Haber-Bosch process that is accounted for 1-2% of the world's energy supply [4]. However, even a 5% decline of ammonia production by the Haber-Bosch process might save 50 TWh [5]. Therefore, the recovery of ammonium from alternative resources significantly contributes to economic and environmental sustainability.

Meanwhile, wastewater has been recognized to be a potential source of nitrogen [6,7]. One of the advantages of municipal wastewater to be used for the recovery of nitrogen compounds is the presence of nitrogen in the form of soluble, inorganic ammonium, and nitrate. Therefore, these compounds can be removed with the available technologies without additional pretreatment (e.g. hydrothermal) to convert the organic nitrogen into the inorganic form for easy capture by plants [8]. However, a rather low nitrogen concentration in municipal wastewater might results in limitations for the recovery process [9]. Consider, the possibility of ammonium-based fertilizer production from highly concentrated ammonium water streams [10], pre-concentration of nitrogen compounds might be needed. Nevertheless, the current wastewater treatment technologies [11], summarized and illustrated in **Fig. 1.,** focus on ammonium removal or turning into nitrate via nitrification, instead of recovery with the further perspective to use. Recently, a few studies have

reported on the ammonium recovery from wastewater by an anaerobic/ion exchange system [12] and selective sorbents [13,14]. Therefore, there is a huge demand for the development of novel approaches focusing on ammonium recovery from municipal wastewater.

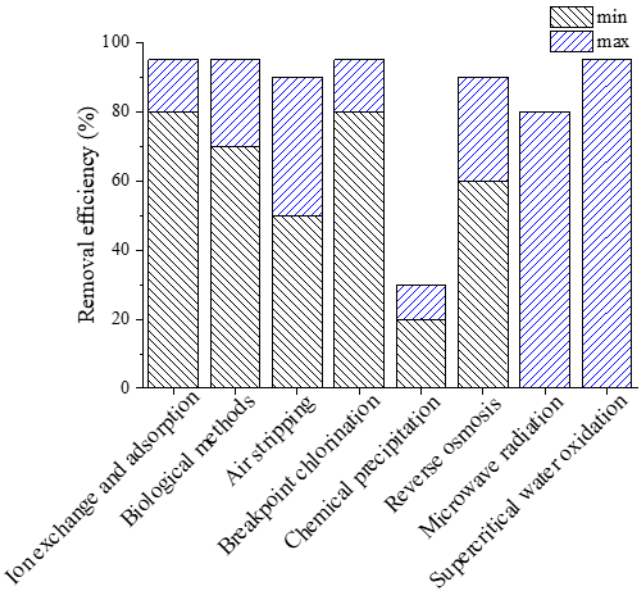

Fig. 1. Technologies for ammonium removal from water and wastewater (modified from [11]).

In this study, we investigated the feasibility of capacitive deionization (CDI) as an emerging technology to be applied to ammonium recovery. CDI is an electrochemical water treatment technology based on the accumulation of oppositely charged ions in the electrochemical double layer (EDL) on the surface of porous electrodes [15]. It is a cyclic process involving electrosorption and desorption of ions by applying and eliminating (or reversing) the applied electric field, respectively. The electrosorption stage is accompanied by the removal of ions from the water stream, resulting in water treatment or desalination while the recovery of the accumulated ions is achieved in the desorption stage. Meanwhile, CDI is known as a desalination technique [16], in which the electrosorption operating principle makes it applicable to the removal of different ions [17–19]. Recently, a few studies reported ammonium removal from synthetic

wastewater by AC cloth [20] and graphene-based [21] electrodes. Additionally, membrane (MCDI) and flow-electrode (FCDI) CDI systems were developed for ammonium removal and recovery [3,22–24]. However, ammonium removal and recovery from municipal wastewater by CDI in a single-pass mode have not been investigated so far.

Activated carbon (AC) is a typically used material for the fabrication of CDI electrodes due to its excellent conductive and sorption properties, high specific surface area, and comparatively low cost [25]. Modification of AC with oxygen functionalities is a confirmed method to improve the electrosorption performance [26,27]. The high sorption capacity of oxygen functionalized materials to cations from aqueous solutions was shown in the literature recently [28,29]. Moreover, recent research demonstrated the formation of bonds between oxygen functionalities and ammonium ions [10]. Within this work, we functionalized AC with oxygen groups by acid treatment providing the generation of (carboxylic (C(=O)OH), lactone (-(C=O)-O-), and phenolic hydroxyl (C_6H_5-OH) groups) on the surface of the material.

In this research, the enhanced ammonium removal and recovery process via the integration of the oxygen functionalized AC (AC-ox) electrode in the CDI cell was presented. Herein, symmetric (pristine AC electrodes) and asymmetric (pristine AC anode + AC-ox cathode) CDI cells were tested under similar conditions and compared for the ammonium removal and recovery from municipal wastewater. Additionally, the electrochemical behavior and electrical energy consumption of the symmetric and asymmetric CDI cells were investigated.

2. Materials and methods

2.1.Chemical reagents

Powdered activated charcoal (Norit A Supra) and hydrochloric acid (HCl, 37%) were obtained from VWR. Poly(vinylidene fluoride) (PVDF, M.W.=534,000), anhydrous N-N-dimethylacetamide (DMAc, 99.8%), nitric acid (HNO_3, 65%), ammonium chloride (NH_4Cl, 99.99%), sodium chloride (NaCl, 99.5%) and sodium hydroxide (NaOH, ≥97.0%, pellets) were purchased from Sigma Aldrich. Working solutions were prepared by dissolving the desired amount of salts in ultrapure (Milli-Q) water. Municipal wastewater from Kenkäveronniemi WWTP (Finland) was used for the real-case experiments.

2.2.Oxidation of the activated carbon

Oxidation of the pristine AC was conducted in line with the procedure described before in the literature [2]. Firstly, AC was sequentially washed with boiling ultrapure water and 0.1 M HCl solution to remove impurities from the pores. Then AC was rinsed with ultrapure water until the pH was neutral. After washing, AC was collected from the paper filter and dried in a vacuum oven at 60 ˚C for 4 h. Secondly, the oxidation was conducted by the overnight stirring of washed AC (2 w.t.%, solid content of the suspension) in 5 M HNO_3. Finally, AC-ox was carefully washed with ultrapure water to remove acid residues and then dried in a vacuum oven at 60 ˚C for 4 h.

2.3.Electrodes fabrication

Porous carbon electrodes were fabricated from the pristine AC and AC-ox. The ratio of a polymeric binder (PVDF) was decreased from the recommended 10% to 7% for this study. The comparison of the electrodes containing 10 and 7% of PVDF is illustrated in **Fig. S1.** Mixtures of carbon materials and 7 wt.% of PVDF were blended with the desired volume of DMAc solution

to get a carbon slurry of 38 wt.% solid content. The mixtures were rapidly stirred for 6 h to obtain homogeneous carbon slurries. Titanium plates (7×4×0.2 cm), which served as a current collector, were covered with the carbon slurry using a manual wet film applicator. The electrodes were firstly dried in the conventional oven at 60 °C for 2 h, and then in the vacuum oven at 50 °C overnight. The average mass of the fabricated carbon electrodes was determined to be 120 ± 10 mg, while the average thickness was about 200 ± 20 μm. Prepared electrodes were washed with ultrapure water under flow-through mode before the experiments.

2.4.Material characterization of the electrodes

The specific surface area and the porosity of the pristine AC and prepared electrode materials were calculated through N_2 adsorption-desorption isotherms obtained at 77 K using Micromeritics Tristar II. Samples were degassed overnight at 70 °C to remove moisture before the adsorption measurements. The surface area and average pore diameter were determined according to the Brunauer-Emmett-Teller (BET) model. The total pore volume was deduced using the single point at the adsorption branch of the nitrogen isotherm at $p/p^o = 0.95$. Micropore volume and pore diameter were quantified using the t-plot method. The micropore size distribution was determined by applying the Horvath-Kawazoe (HK) method. X-ray powder diffraction (XRD) has been applied to evaluate the crystalline structure of the material using a high-resolution Empyrean diffractometer (PANalytical). XRD diffractogram was recorded utilizing Co Kα radiation at a voltage of 40 kV from 10° to 120° 2θ angles. Fourier-transform infrared spectroscopy (FTIR) has been conducted to identify the surface functionalities of AC before and after oxidation. FTIR spectra were obtained at 4 cm^{-1} resolution from 400 to 4000 cm^{-1} at a rate of 100 scans per sample using Bruker Vertex 70. Rubber band baseline correction (OPUS, Bruker) was applied to FTIR spectra. The surface morphology of the prepared materials was determined by scanning electron

microscopy (SEM) using Hitachi S-4800. The wettability of the electrode surface was evaluated by the contact angle (CA) measurements using the OCA 15 EC instrument. Determination of the surface charge of the tested materials was conducted in the suspension of 0.1 M NaCl solution with a solids content of 0.1 g/L using ZetaSizer Nano ZS ZEN 3500 (Malvern Instruments Ltd.).

2.5.Electrochemical experiments

The electrochemical measurements were conducted using OctoStat5000 potentiostat (Ivium). The electrodes were examined by cyclic voltammetry (CV) and galvanostatic charge-discharge (GCD) using two- and three-electrode cells. Measurements in a two-electrode cell were conducted using the described symmetric and asymmetric CDI cells equipped with a glassy fibrous separator, saturated with the electrolyte (1 M NaCl). The electrodes were of a similar mass (0.11 g). Measurements in a three-electrode cell were carried out in 1 M NaCl continuously bubbling with nitrogen. A platinum wire and Ag/AgCl electrode were employed as counter and reference electrodes, respectively. Glassy carbon (GC) electrode was used as the substrate for the working electrode. The GC electrode was pre-treated with ethanol and then dipped in the carbon slurry. The prepared working electrodes were dried in the conventional oven at 60°C for 2 h and under vacuum at 50°C overnight. The mass of 0.28 cm^2 carbon coverage obtained onto GC electrodes was 0.0030 g for the pristine AC and 0.0027 g for the AC-ox, which was equivalent to about 0.1 mm in thickness. The working electrodes were initially pre-treated using CV at 10 mV/s in the chosen potential range in 1 M NaCl until stable voltammograms were obtained.

Specific capacitance $Cs_{(CGD)}$ (F/g), determined by GCD in two-electrode cell was calculated by Eq.1 [30]:

$$Cs_{(GCD)} = \frac{I \cdot dt}{dV \cdot m} \quad (1)$$

where I is the constant current (A), dV/dt is calculated from the slope of the discharge curve, m is the total mass of the active material in both electrodes (g).

Specific capacitance $Cs_{(CV)}$ (F/g), determined by CV in both cell configurations was calculated by the equation Eq.2 [30]:

$$Cs_{(CV)} = \frac{I}{v \cdot m} \quad (2)$$

where I is the average current (A), v is a scan rate (V/s), and m is the total mass of the active electrode material (g).

2.6. CDI experiments

The CDI experiments were carried out in a single-pass mode using a flow-by cell with the inner working volume of 1 cm^3 at 2 mL/min flow rate and 1.2 V applied potential difference. The flow channel between two electrodes was constructed employing a silicone gasket of 1 mm thickness. The discharging of the electrodes was conducted via short-circuiting. The CDI cycle lasts for 1000 s. The charging/ discharging stages were adjusted to 500 s. The configuration of the CDI cell and the identification of the optimal operation parameters were reported in the literature [31]. The symmetric CDI cell was composed of a pair of pristine AC electrodes, whereas, the asymmetric CDI cell consisted of the pristine AC anode and the AC-ox cathode for the enhanced NH_4^+ removal. A fresh pair of electrodes was used for every single test to eliminate the effect of incomplete regeneration of the electrodes on the results.

To compare the electrosorption and desorption performance of the pristine AC and AC-ox electrodes, 5.5 mmol/L NH_4Cl solution (pH 5.4) was used. Working solutions contained 0.55,

1.38, 2.77, and 5.55 mmol/L of NH_4^+ ions were used to estimate the effect of the initial concentration on the electrosorption performance of electrodes. The long-term CDI operation was carried out for 50 continuous cycles in a 5.5 mmol/L NH_4Cl solution to investigate the stability and repeatability of the process. The CDI cells were paused and flushed with DI water between the runs. The samples of municipal wastewater were collected from the primary clarifier and filtered with a vacuum pump equipped with a cellulose-acetate (0.45 um) filter before the CDI experiments. The composition of the wastewater used in this study is summarized in **Table S1.** The performance of the AC-ox electrode for NH_4^+ ions removal and recovery was investigated in the presence of competitive ions.

Single-pass conductivity and pH measurements were recorded every 30 s by a multiparameter (InoLab Multi 9620 IDS, WTW GmbH). Samples for the concentration measurements of NH_4^+ ions were taken every two minutes and were analyzed by ion chromatography (Shimadzu), equipped with IC YS-50 (Shodex) column for cation determination. Competitive ions present in wastewater samples were detected by inductively coupled plasma optical emission spectrometry (Agilent Technologies 5110 ICP-OES). The measurements of the concentration of the ions were conducted at the following wavelength: 766.491 nm (K^+), 568.821 nm (Na^+), 422.637 nm (Ca^{2+}), 285.213 nm (Mg^{2+}).

The electrosorption capacity (Q, mmol/g) and ions removal efficiency (η, %), used to assess the CDI performance, were calculated by Eq.3 and 4, respectively [32]. Desorption capacity and ions recovery efficiency were calculated based on the differences in the solution concentration at the discharge stage and initial concentration.

$$Q = \frac{\left(\int_{t_0}^{t_s}\left(\frac{C_0 - C}{t}\right)dt\right)\cdot v\cdot(t_s - t_0)}{m} \quad (3)$$

$$\eta = \left(\int_{t_0}^{t_s} \left(\frac{C_0 - C}{C_0 t} \right) dt \right) \cdot 100\% \quad (4)$$

where C_o and C (mmol/L) are the initial concentration and the concentration of the solution at time t, υ (L/s) is the flow rate, m (g) is the mass of AC material in the electrodes, t_0 and t_s (s) are the initial and saturated time, respectively.

The electrosorption selectivity of the fabricated electrode for one ion over another was calculated by Eq.5 [33]:

$$S_{A/B} = \frac{\frac{c_{ads,A}}{c_{ads,B}}}{\frac{c_{m,A}}{c_{m,B}}} \quad (5)$$

where $S_{A/B}$ is the selectivity coefficient for species A over species B, $c_{ads,A}$ and $c_{ads,B}$ are the adsorbed concentrations of species A and B, respectively; $c_{m,A}$ and $c_{m,B}$ are the mobile concentration of species A and B, respectively.

The energy consumption (W, kWh/mmol) required for the removal of target ions was calculated by Eq.6 [8]:

$$W = \frac{E}{V \cdot (C - C_0)} \quad (6)$$

$$E = \frac{U \cdot \int_0^t I dt}{3600} \quad (7)$$

where E is the energy consumption (kWh), C_o and C (mmol/L) are initial and final concentrations, V is the volume of the solution (L) passed through the CDI cell in one operating cycle, I is the current (A) for the operation time, and U is the applied voltage (V).

The charge efficiency (Λ, %) at one cycle was determined following Eq.8 [34]:

$$\Lambda = \frac{Q}{\mathrm{M}} \cdot \mathrm{m} \cdot \frac{F}{\int_{t1}^{t2} I dt} \quad (8)$$

where Q (mg/g) is the electrosorption capacity at one cycle, M – is the molecular weight of NH_4Cl (mg/mmol), m (g) is the weight of AC material in the electrodes, F – is the faradaic constant (96485 C/mol).

3. Results and discussion

3.1.Material characterization of the pristine AC and AC-ox electrode materials

N_2 adsorption/desorption isotherms of pristine AC and its modifications are shown in **Fig. 2 (A, D) (insets)**, and the textural properties are summarized in **Table S2**. N_2 adsorption/desorption isotherms of carbon materials are a combination of Type I and II isotherms with a type H4 hysteresis loop according to IUPAC classification [35]. Therefore, tested carbons can be characterized as a combination of non- and microporous materials with narrow slit pores. The presence of a hysteresis loop indicates slower desorption corresponding to the changes of the pore structure [36]. The increase in the size of the hysteresis loop aligns with the successive modifications of the pristine AC. The oxidation of the material with nitric acid resulted in the filling of the pores owing to the generated oxygen functionalities [37] along with the destruction of pore walls [2] leading to the decrease in the surface area. Besides, the decline in the surface area of the fabricated carbon electrode materials is attributed to clogging the pores of the material by the polymeric binder [38]. Thus, the specific surface area (SSA) of pristine AC was determined to be 1760 m^2/g, while the SSA of the AC-ox was decreased to 1573 m^2/g. The SSA of the electrode materials, prepared from pristine AC and AC-ox was further decreased down to 555 m^2/g and 325 m^2/g, respectively. The size distribution of the micropores (**Fig. 2 (A, D)**) was determined by the

HK method assigned to slit pore geometry. Narrow pore size distribution around 0.5 – 0.6 nm was observed for pristine AC and AC-ox. There were no distinct changes in the micropore volume of AC after oxidation. However, a dramatic decrease in micropore volume (from 0.33 to 0.02 cm^3/g) was observed for the prepared carbon electrode materials. Pore size distribution plots based on the BJH model (**Fig. S2)** confirmed the presence of a small number of mesopores (3 – 4 nm) for the tested carbon materials.

The X-ray diffractogram of the pristine AC and AC-ox is represented in **Fig. S3.** Amorphous halo around 24–32° indicates the poor crystallinity of the materials. There were no changes observed in the crystalline structure of the material after the oxidation process. The acquired peak at 51° and a broad peak at 95° indicate a graphitic carbon, distinctive for all AC-based materials [39].

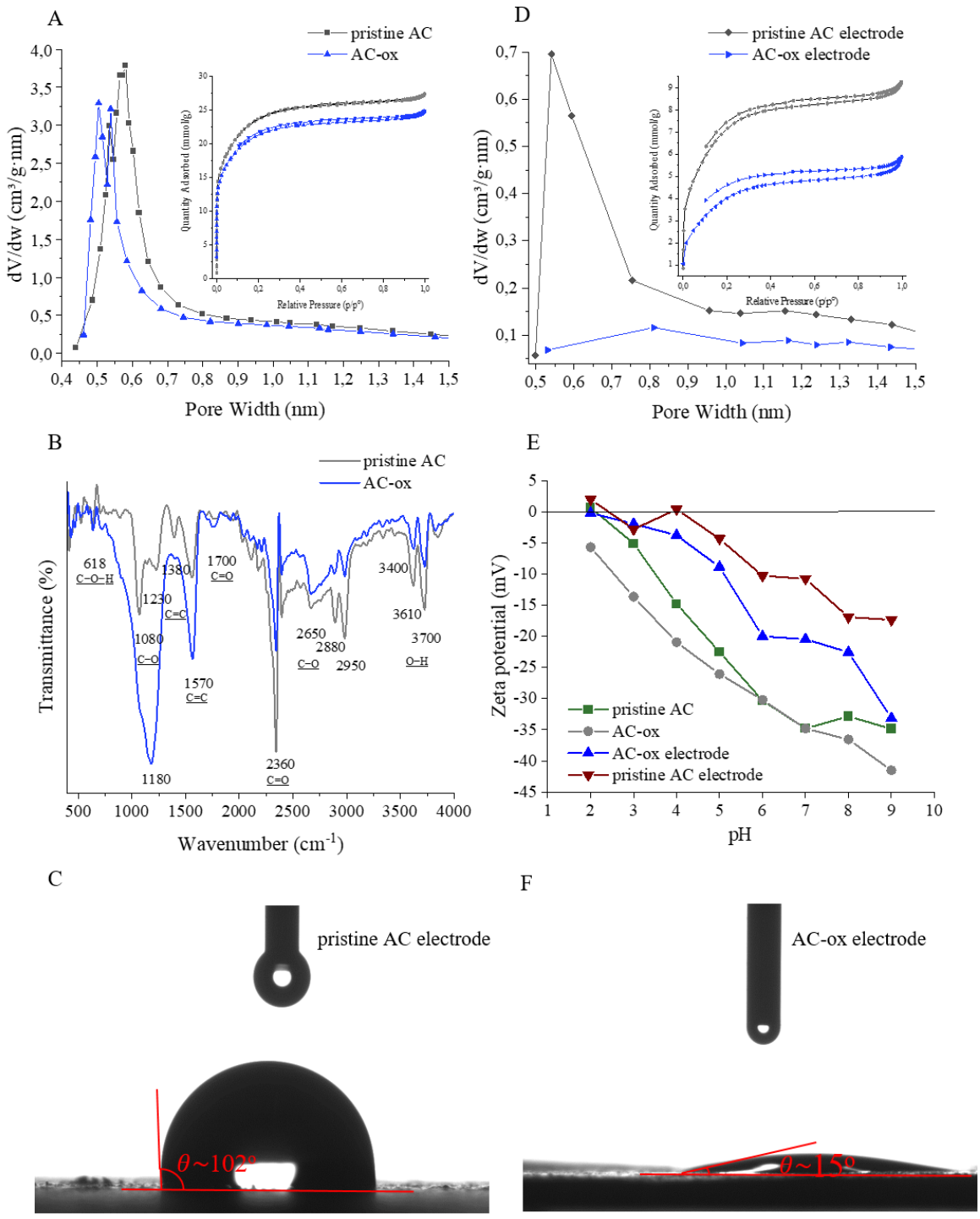

Fig. 2. HK pore size distribution and N_2 adsorption/desorption isotherms (insets) of (A) pristine AC and AC-ox, and (D) AC electrode materials. (B) FTIR spectra of pristine AC and AC-ox. (E) Zeta potentials as a function of pH in 0.1 M NaCl. The contact angle of a water droplet on the surface of (C) pristine AC and (F) AC-ox electrodes at the initial moment.

The FTIR spectra of pristine AC and AC-ox are shown in **Fig. 2 (B)**, while peak assignments are summarized in **Table S3**. Both spectra of pristine AC and AC-ox demonstrate similar patterns. However, the changes in the transmittance of FTIR peaks were observed indicating changes in the content of functional groups on the surface of the materials [40]. A broad peak at 1180 cm^{-1} of AC-ox spectra, merging the bands at 1080 cm^{-1} and 1230 cm^{-1} in pristine AC spectra, indicates the increase in the amount of C-O single bonds, characteristic for ethers, phenol, and acids [41,42], attributing to the acid treatment. In line with the oxidation of the AC, the increase of a peak at 1700 cm^{-1}, corresponding to C=O stretching vibrations in conjugated aromatics, was observed. The decrease of a peak transmittance at 1380 cm^{-1} indicates the deformation of C=C in phenols while the strong peak at 1570 cm^{-1} corresponds to C=C stretching in highly conjugated carbonyl groups [41]. The sharp peak at 2360 cm^{-1} is assigned to C=O asymmetric stretching [43]. A band of peaks at 2650 cm^{-1}, 2880 cm^{-1}, and 2950 cm^{-1} is related to C-H stretching in ($-CH_2$) and ($-CH_3$) groups in aliphatic hydrocarbons [42,44,45]. Peaks in a range of 3400-3700 cm^{-1} indicate O-H stretching vibrations in H_2O [44]. A small peak at 618 cm^{-1} is attributed to C-O-H twist bending vibrations [46]. The presented results of FTIR spectra demonstrate the increase in oxygen functionality of the oxidized carbon.

According to Zeta potential measurements, represented in **Fig. 2 (E),** AC originally has a negative surface charge. Oxidation of AC promotes the increase of the negative surface charge, while the polymeric binder (PVDF), added to the electrode composition, oppositely contributes to the decrease of the negative surface charge. Pristine AC and AC-ox have the same zeta potential of -34.8 mV at pH 7. However, the AC-ox electrode material demonstrated higher negative zeta potential (-22.55 mV) at pH 7 compared to pristine AC electrode material (-16.9 mV). Therefore,

the higher negative surface charge of the AC-ox electrode material should facilitate the electrosorption of cations.

A surface wettability test was conducted to investigate the effect of oxidation on the hydrophilicity of the electrode material. Acid treatment contributes to the growth of surface hydrophilicity due to the reduction of the mineral content [47]. **Fig. 2 (C, F)** represents the images of water droplets onto the surfaces of the electrodes at the initial moment. The CA of a droplet onto the pristine AC electrode was determined to be 102°. Moreover, the observed permeation time for the water droplet into the pristine AC electrode was 38 min (**Fig. S4**). In contrast, the CA of a water droplet onto the AC-ox electrode was found to be 15° in the beginning, and then it was completely spread over the surface. Therefore, the hydrophilicity of the oxygen functionalized material dramatically increased in comparison to the pristine AC. The hydrophilic surface of the material facilitates the permeation of the solution into the electrode, thus contributing to the acceleration of the electrosorption efficiency. In general, the high hydrophilicity of the material is beneficial for the CDI process [32,48].

Prepared AC electrodes represent a highly porous and irregular surface morphology as depicted in **Fig. S5 (A, B)** and **S6 (A, B)**. SEM images (**Fig. S5 (C, D)** and **S6 (C, D)**), obtained at higher magnification (25 k), demonstrate the rock-like shape of AC particles. Moreover, no particles from the polymeric binder were observed, in line with the observations from our previous research [31]. As a result of the known clogging effect of the polymeric binder on pores, the decrease in the ratio of PVDF was beneficial for the electrode composition. Meanwhile, no changes in electrode behaviour were noticed. The AC electrodes maintain durability even after continuous operation. The atomic elemental composition of the electrode materials was determined by EDS in parallel with SEM imaging (**Table S4** and **S5**).

The differences in material properties caused by the oxidation of AC were investigated. The effect of the increase of the oxygen functionalities, identified with FTIR spectroscopy, was also observed from the CA measurements. Consequently, the surface of the AC electrode was developed with increased hydrophilicity and added functional sites. Additionally, the AC-ox obtained a more negative surface charge resulting in stronger electrosorption of positively charged ions. However, there were no changes in the crystalline structure and morphology of AC detected after the acid treatment. Nevertheless, the distinct changes in the surface properties accompanied by the oxidation of AC and electrode preparation were noticed. The addition of the polymeric binder demonstrated a greater effect on the reduction of the specific surface area in comparison to the oxidation procedure. Considering the significance of the specific surface area for the electrosorption and electrochemical performance of the electrode materials, the further development of the porous carbon electrodes without losing the high porosity value should be considered in future studies.

3.2.Electrochemical performance of pristine AC and AC-ox electrodes

The electrochemical performance and charge storage mechanism of the prepared electrode materials has been investigated by CV. Charging/discharging stability was examined by GCD. An electrochemical study of the prepared electrodes has been conducted in two- and three-electrode cells. Data, obtained from the two-electrode configuration, provides information about the factual electrochemical behavior of the cell. While capacitive or pseudocapacitive behavior of a single electrode might be investigated in the three-electrode cell [49].

The potential range of any electrode, available for study the electrochemical reactions, is limited by the potentials of these reactions, associated with the electrolyte type and the electrode material. In the three-electrode cell, cathodic and anodic limits have been selected according to the

potential window of the aqueous electrolytes (1 V), and the overpotentials of carbon electrodes, observed at - 0.4 V and 1.2 V, respectively [50]. In the two-electrode cell, CV curves have been recorded using the operating potentials of CDI (0 and 1.2 V)

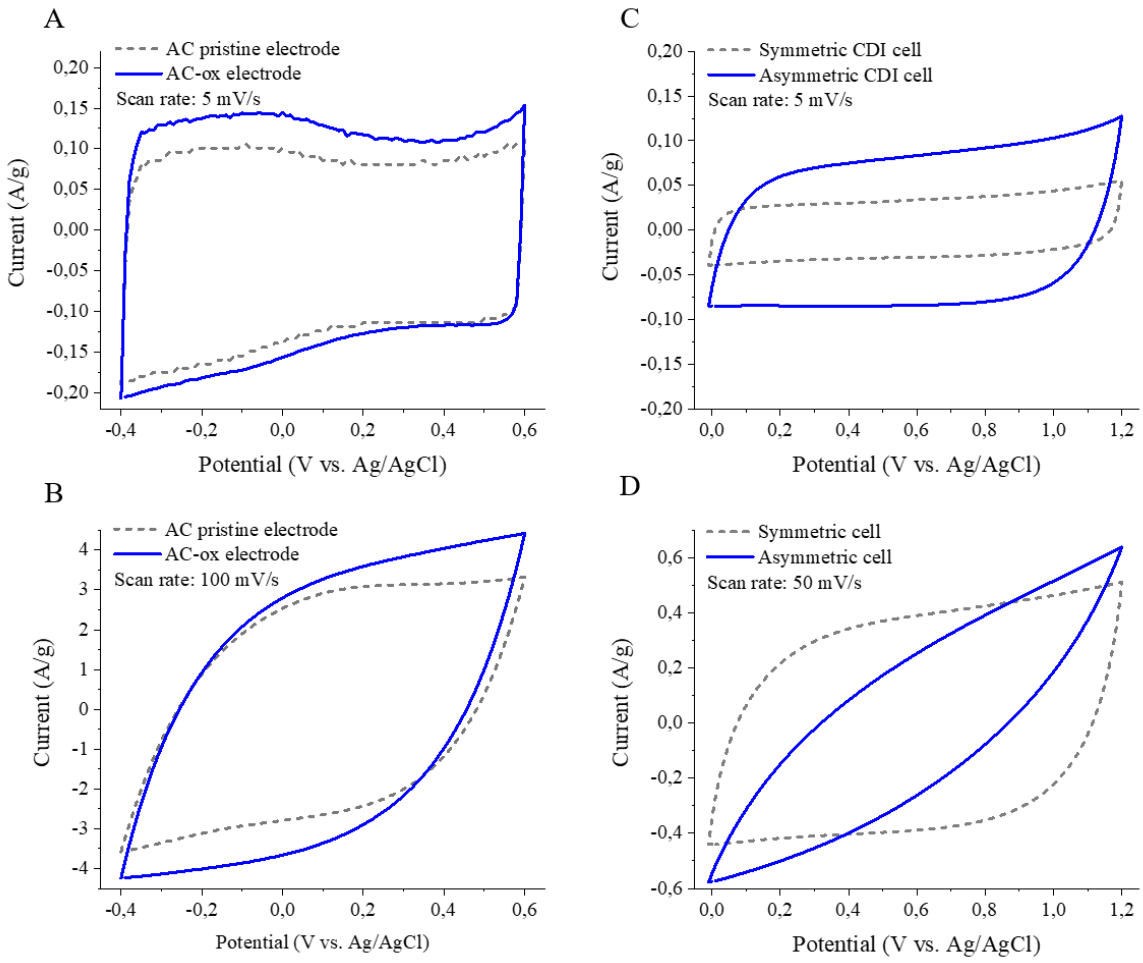

Fig. 3. CV curves obtained in the three-electrode cell (A) at 5 mV/s and (B) at 100 mV/s for AC pristine and AC-ox electrodes. CV curve obtained in the two-electrode cell (C) at 5 mV/s and (D) at 50 mV/s.

CV profiles, recorded from AC pristine and AC-ox electrodes at 5 mV/s **Fig. 3(A)**, exhibit a quasi-rectangular shape, related to a capacitive behavior of the electrodes. While the humps in the cathodic area indicate redox reactions on the electrode surface [51]. The higher hump on the CV curve and the larger sweep area of the AC-ox electrode profile are associated with the added oxygen-containing functional groups. However, the CV profiles from the two-electrode cell **Fig.**

3(B) show a quasi-rectangular shape with neither oxidation nor reduction peaks. Only a little inflection, observed at 1.2 V, indicates the beginning of water splitting. Thus, the influence of oxygen functionalities on the electrochemical behavior is hidden in the case of the measurements in a full cell. Nonetheless, with the increase of the scan rate, CV profiles tend to be a leaf-like shape, as illustrated in **Fig. S7 and S8**, pointing out the rise of instability of EDL and pseudocapacitive nature of the electrodes [52]. Interestingly, the AC pristine electrode and the symmetric cell keep a quasi-rectangular shape beyond the increasing scan rates, as represented in **Fig. 3(B, D)**. Therefore, the recorded CV profiles demonstrate the capacitive-Faradaic process [53], inherent for both tested electrodes.

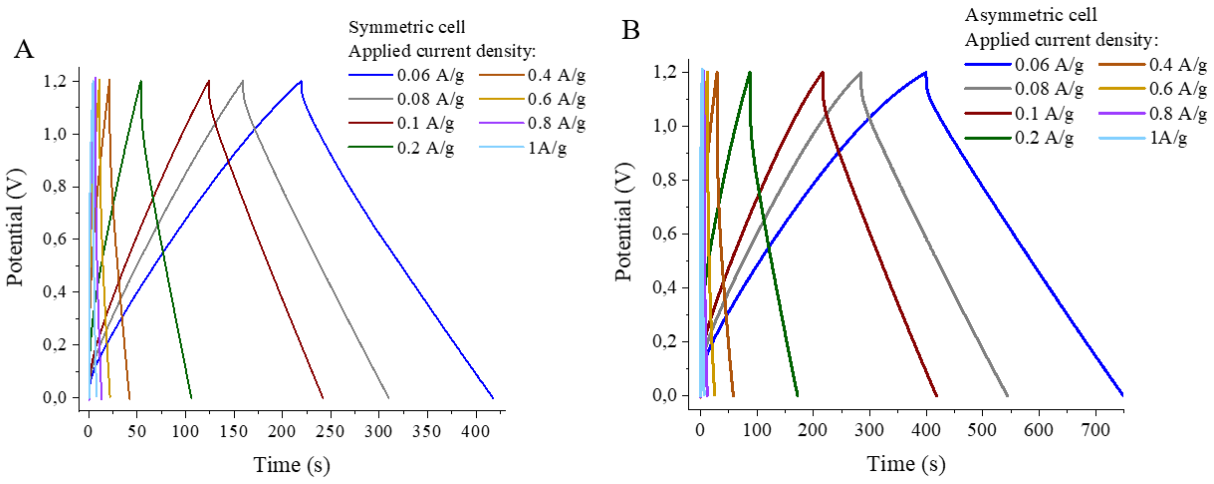

Fig. 4. GCD curves for (A) symmetric and (B) asymmetric cells at different current densities in 1 M NaCl.

GCD measurements were conducted in the two-electrode cell within the potential window of 0 V to 1.2 V **Fig. 4(A, B)**, same as the operating conditions of CDI experiments. The values of the current densities (0.06 – 0.2 A/g) for GCD have been chosen in accordance with the CV. Triangular, and mostly symmetric GCD curves also indicate pseudocapacitive behavior of the electrode materials [51]. Higher current density contributes to shorter cycling time, and the increasing ohmic drop, as illustrated in **Fig. S9.** The increasing ohmic drop is related to the

decreasing equivalent series resistance (ESR) (**Fig. S10**), and therefore to the decline of the resistances of the electrolyte, electrode material, add current collector. Therefore, the desorption of charges from the EDL is faster at higher current densities. Additionally, the cyclic performance of the symmetric and asymmetric cells has been examined. Both cells keep outstanding cyclic stability during 1000 GCD cycles, as shown in **Fig. S11.**

Table 1. The specific capacitance of AC pristine and AC-ox electrodes measured with different cell configurations

Cell configuration	CV		GCD	
	Scan rate, mV/s		Current density, A/g	
	1	100	0.06	1
AC pristine electrode (three-electrode cell)	11.5 F/g	0.16 F/g	-	-
AC-ox electrode (three-electrode cell)	13 F/g	0.09 F/g	-	-
Symmetric cell	2.8 F/g	0.08 F/g	10.4 F/g	6.0 F/g
Asymmetric cell	8.6 F/g	0.05 F/g	18.3 F/g	6.1 F/g

The boundary values of specific capacitance of the tested electrodes, obtained from CV and GCD measurements in two-and three-electrode cells, are summarised in **Table 1.** AC-ox electrode and the asymmetric cell demonstrate higher specific capacitances at lower values of the scan rate, compared to the AC pristine electrode and the symmetric cell. This might be related to the occurrence of oxygen-containing functionalities, observed at a moderate scan rate [49]. While with the acceleration of the rate of CV recordings, the influence of redox reactions becomes neglectable because of the ion diffusion limits [54], and both tested electrodes represent similar capacitance (**Fig. S12(A, B**)). The values of specific capacitance, obtained in the two-electrode cell via GCD are considered more reasonable [55]. Nevertheless, a similar dependence has been observed for the specific capacitance and the current density, associated with the limited speed of ions to diffuse into the electrode interface. The asymmetric cell demonstrates the higher specific capacitance, compared to the symmetric cell, at the low levels of the current density. While with the rise of the current density, the values of the specific capacitance of the symmetric and

asymmetric cells become similar (**Fig. S12(C**). Therefore, the positive influence of the added oxygen functionalities, observed at low rate CV and GCD, on the electrochemical behavior of the electrodes, has been observed for the AC-ox electrode and the asymmetric cell.

3.3. Electrosorption performance of pristine AC and AC-ox electrodes

Electrosorption performance of the pristine AC and AC-ox electrodes were compared in a 5.5 mmol/L NH_4Cl solution. Electrosorption profiles of the pristine AC and AC-ox electrodes are illustrated in **Fig. 5 (A).** Although the stable cyclic performance of both electrodes, the AC-ox electrode demonstrated higher electrosorption and desorption performance in comparison to the pristine AC electrode. In addition, the long-term CDI operation has been carried out to investigate the stability and repeatability of the CDI process. Plots illustrated the long-term CDI operation (during 50 cycles), are presented in **Fig. S13(A).** The relevant potential application (charge/discharge) and the current response are demonstrated in **Fig. S13(B).** The stable, repetitive performance of the electrodes was observed during the continuous operating cycles in every run. However, the decrease of the electrosorption performance and the electric current response were observed in every new run after the operation shutdowns.

The changes in the concentration of NH_4^+ ions are illustrated in **Fig. 5 (B)**. Removal of NH_4^+ ions by the AC-ox electrode was determined to be around three times more effective in comparison to the pristine AC electrode. The decrease in the electrical conductivity of the solution and the concentration of NH_4^+ ions are aligned with the decline of the electrical current response, caused by the applied potential (**Fig. 5 (C)**).

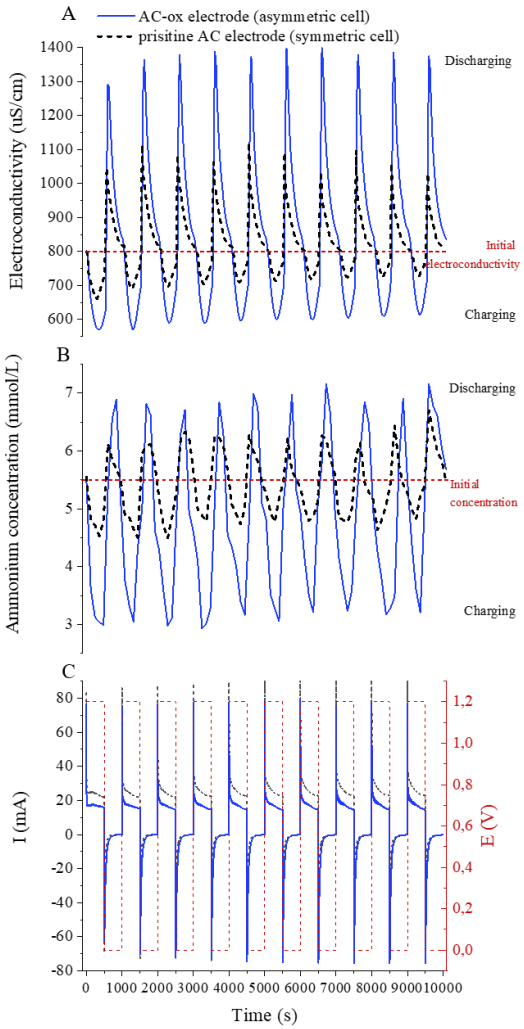

Fig. 5. (A) Electroconductivity and (B) concentration profiles, (C) the electrical current response of the symmetric and asymmetric CDI cells operated under 1.2 V (charge) and 0 V (discharge) in a 5.5 mmol/L NH_4Cl solution at sequential charging/discharging cycles.

Despite the stable CDI performance, the decline of NH_4^+ ions removal efficiency was observed after the first operation cycle (**Fig. 6 (A)**). The removal efficiency of pristine AC and AC-ox electrodes at the first operational cycle was calculated to be 30% and 83%, respectively, whereas the overall average removal efficiency decreased to 22% for the pristine AC electrode and 63% for the AC-ox electrode. The electrosorption capacities of NH_4^+ ions by the pristine AC and AC-ox electrodes were 0.24 mmol/g and 0.67 mmol/g, respectively, during the first operation cycles **(Fig. 6 (B)**). The average electrosorption values were calculated to be 0.18 mmol/g for the

pristine AC electrode and 0.47 mmol/g for the AC-ox electrodes. The overall average recovery efficiency of pristine AC and AC-ox electrodes was calculated to be 12% and 21%, respectively. Therefore, ammonium recovery efficiency for the AC-ox electrode was estimated to be around two times higher compared to the pristine AC electrode **(Fig. 6 (C))**. Moreover, the recovery efficiency of the fabricated AC-ox electrode in our study is higher compared to the 5-13% recovery obtained with the saturated hydrochar [10]. The desorption capacity of NH_4^+ ions (**Fig. 6 (D)**) was 0.16 mmol/g at the first operating cycle and averaged 0.12 mmol/g by the pristine AC electrode. The AC-ox electrode showed the desorption capacity towards NH_4^+ ions of 0.32 mmol/g at the first operating cycle, 0.25 mmol/g at average.

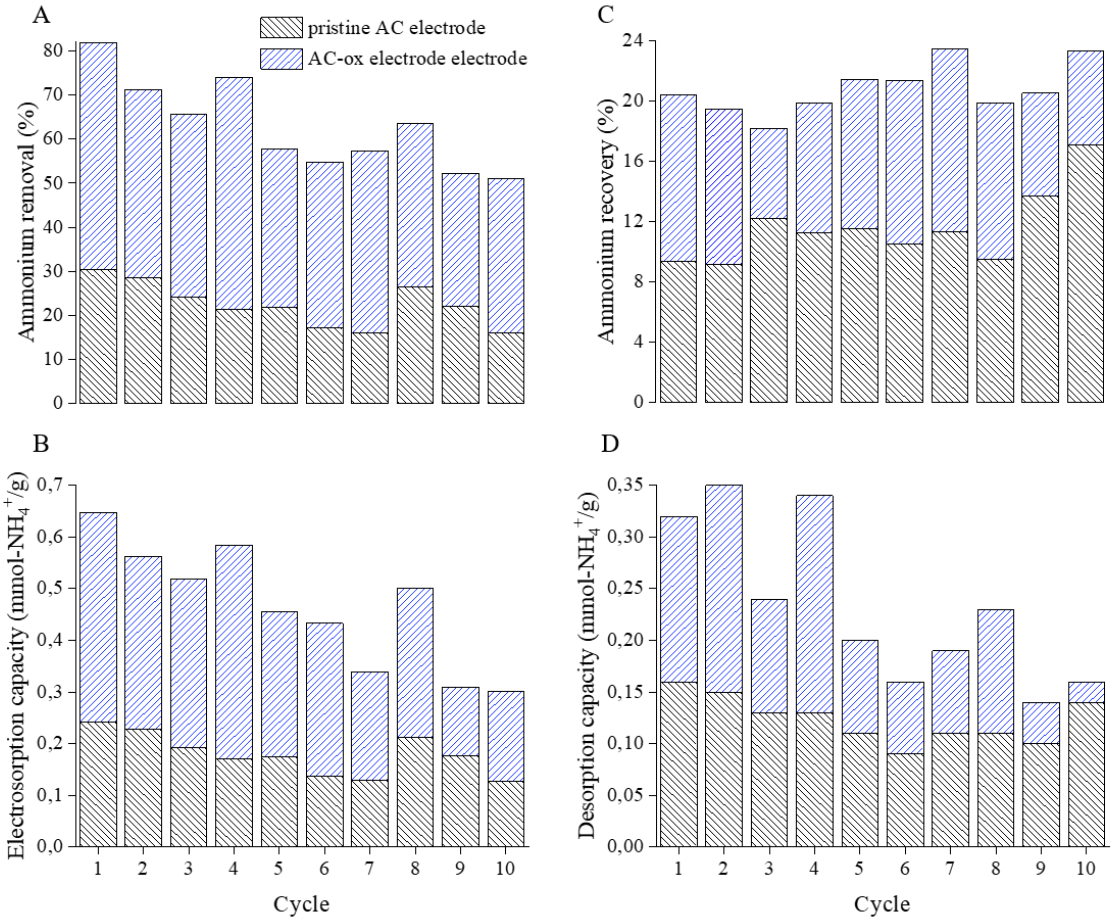

Fig. **6**. (A) Removal efficiency, (B) electrosorption capacity, (C) recovery efficiency, and (D) desorption capacity of the pristine AC and AC-ox electrodes towards NH_4^+ ions at consecutive operating cycles.

The mechanisms occurring at the surface of the electrodes during the repetitive cycles affect the recovery and removal efficiencies of the electrodes [56]. Increased recovery efficiency is observed with the increase in the number of operating cycles because of decreased ion retention capability of the electrodes over a long time. Since the electrodes remain slightly polarised during the discharge, incomplete desorption of ions occurs [57]. Therefore, fewer active sites are available for the following operating cycles. Owing to this, electrically conductive porous materials with high regenerability are needed to be developed to support the CDI process.

The profile of the electrical current response of the symmetric and asymmetric CDI cells, obtained under the constant voltage charge/discharge, is illustrated in **Fig. 5 (C).** An average instantaneous current occurring at the beginning of the charging and discharging stages of the symmetric CDI cell was detected to be 88 and -73 mA, respectively. On the other hand, an average instantaneous current in the asymmetric CDI cell was 77 mA at the beginning of the charging stage and -73 mA at the beginning of the discharging stage. The similar peaks of the electrical current response for the charging and discharging cycles indicate the reversibility of the electrosorption performance [58]. The transient current under the applied constant voltage of 1.2 V was detected to be 23 mA and 16 mA for the symmetric CDI cell and the asymmetric CDI cell, respectively. While the charge efficiencies at the first operating cycle were calculated to be 22% for the symmetric cell and 84% for the asymmetric one. **Fig. S15** illustrates fluctuations of the charge efficiency during the cycling process. Since the charge efficiency is low in the symmetric CDI cell, a higher current is derived for the electrosorption [59] to balance the surface electrode charge by counter ions from the solution [60]. This is in line with a disparate current distribution over an

electrode pair in the symmetric cell, while the different charges of the electrodes in the asymmetric cell balance the potential distribution, resulting in enhanced charge efficiency, electrosorption, and cyclability [61]. Besides, the hydrophilicity of the cathode facilitates ionic diffusion and charge transfer in the asymmetric CDI cell [62]. Therefore, the accumulated ions also participate in balancing the applied potential, resulting in the mitigation of the transient current [63]. Higher energy investments, required for the operation of the symmetric cell, are further demonstrated by the energy, consumed for the removal of NH_4^+ ions from monocomponent solution. Thus, the energy consumption of 0.215 kWh/mmol was determined for the symmetric cell, while 0.085 kWh/mmol – for the asymmetric one.

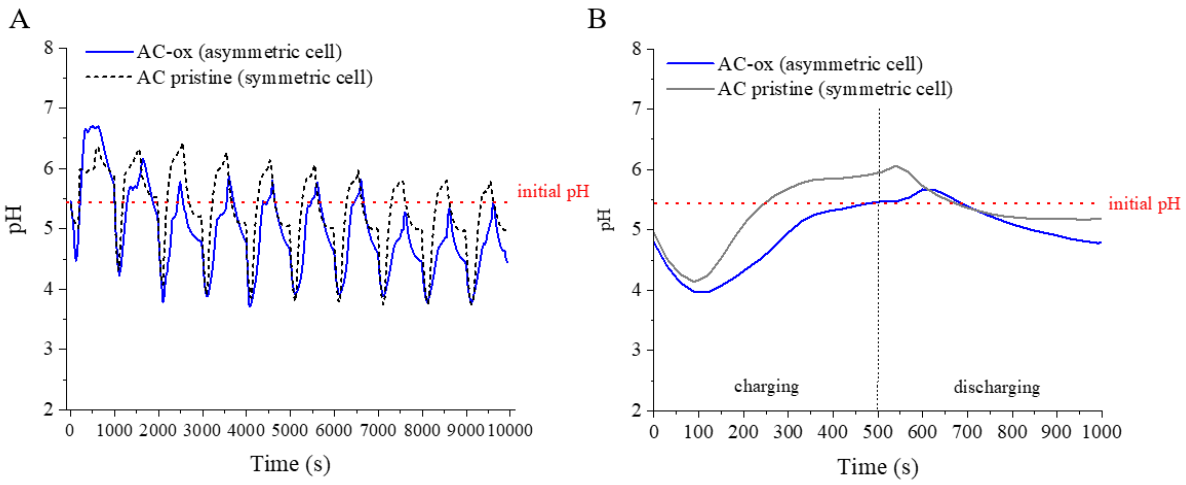

Fig. 7. pH variations during 10 sequential charging/discharging cycles under a constant voltage of 1.2 V (A); averaged pH measurements for one complete operating cycle.

To characterize the CDI performance in terms of the occurrence of redox reactions, pH measurements of the CDI effluent were investigated. **Fig. 7 (A)** displays the variation profiles of pH recorded for ten sequential charging/discharging cycles of the symmetric and asymmetric cells. Both pH profiles demonstrated identical trends: each charging stage was emphasized with the rapid decline of pH regarding the baseline (pH 5.4) in the beginning, and the continuous pH rise with achieving the maximum value in the end. The decrease of pH down to the baseline and lower was

observed at the discharging step. The continuous operating cycles demonstrated the progressively decreased pH fluctuations with a tendency to the acidic region. Averaged pH profiles are presented in **Fig. 7 (B).** It is seen that the minimal pH values of 4.1 and 4.0, and the maximal pH values of 6.0 and 5.7 for symmetric and asymmetric cells, respectively, are associated with the changes of the applied electrical field. Similar pH behaviour was reported by Lado et al. and Zhang et al. [64,65]. Accordingly, pH decrease (from 5.4 to 4.0) occurs because of the release of hydrogen ions during the anodic oxidation of one of the components of the system (carbon electrode, Cl^- ions in feed solution, or oxygen evolution). While a slight pH rise over the baseline might correspond to the reduction of the dissolved oxygen on the cathode. The asymmetric cell demonstrated a smaller increase of pH due to the AC-ox cathode, where available sites were already occupied with oxygen functionalities.

3.4. Ammonium removal and recovery by the AC-ox electrode

3.4.1. Dependence on the initial concentration

The electrosorption performance of the AC-ox electrode depending on the initial concentration of the working solution is illustrated in **Fig. 8 (A).** Complete saturation of the AC-ox electrode by NH_4^+ ions was detected at 480 s after the beginning of the CDI cycle while the highest recovery value was achieved at 840 s. The electrosorption efficiency increased with the increase of the concentration of the tested solution because the solution with the higher ionic strength contributes to the stronger electrical forces in a CDI cell. Therefore, the ions from the concentrated solutions are strongly attracted to the carbon electrodes.

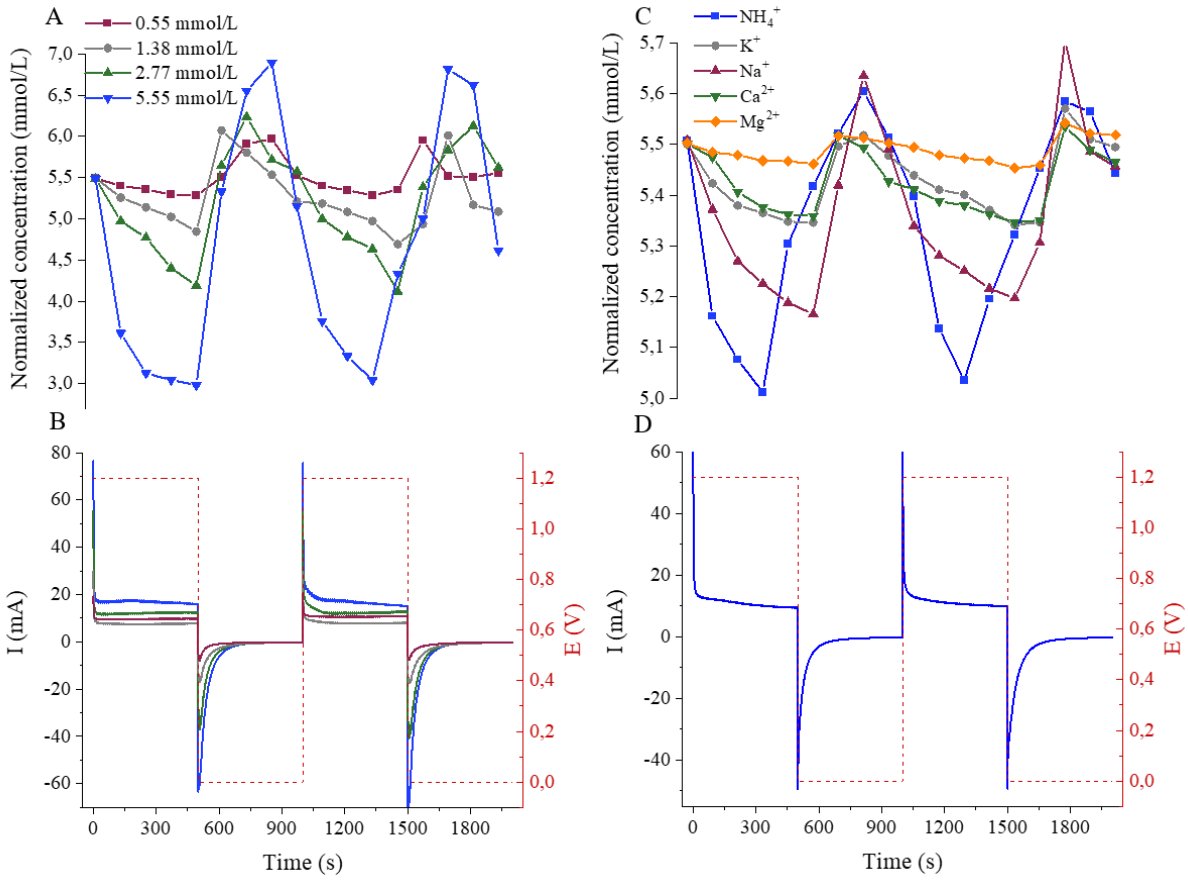

Fig. 8. Electrosorption performance of the AC-ox electrode and electrical current response in the asymmetrical CDI cell (A, B) depending on the initial concentration of NH_4^+ ions and (C, D) in real wastewater.

The value of electrosorption capacity of the AC-ox electrodes for 0.55, 1.38, 2.77, and 5.55 mmol/L of NH_4^+ solutions was calculated to be 0.04, 0.11, 0.23, 0.67 mmol/g, respectively, while the ammonium removal efficiency was estimated to be 53, 54, 57, and 83% in the same order for the tested solutions **(Fig. 9(A))**. A slight decrease in the electrosorption capacity and removal efficiency for different concentrations were observed in the sequential CDI cycles. The electrical current measured in the CDI cell increases with the increase in the electrolyte concentration **(Fig. 8(B))**. However, less energy was consumed per mmol of NH_4^+ ions from more concentrated solutions **(Fig. 10(A)**). Thus, 0.442 kWh/mmol was consumed for 0.55 mmol/L NH_4^+ solution, and 0.092 kWh/mmol was required to operate with 2.77 mmol/L NH_4^+ solution. The recovery

efficiency demonstrated a decline with the increased concentration **(Fig. 9(A)).** The higher concentration provides the low-or reverse-ion concentration gradient between the solution and the surface of the porous carbon electrode that prevents desorption [56]. As a result, ammonium recovery of 46% at 0.55 mmol/L NH_4^+, 29% at 1.38 mmol/L NH_4^+, 21% at 2.77 mmol/L NH_4^+, and 20% at 5.55 mmol/L NH_4^+ was achieved. While, the desorption capacity was calculated to be 0.038, 0.067, 0.075, 0.32 mmol NH_4^+ /g for the increasing concentration of the solution in the same order.

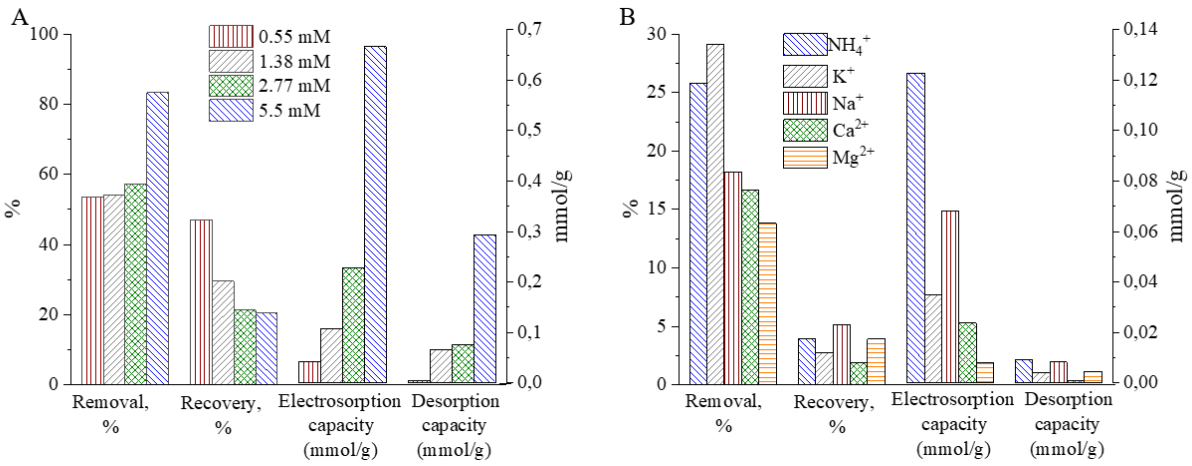

Fig. 9. Removal and recovery efficiencies, electrosorption, and desorption capacities of the AC-ox electrode towards NH_4^+ ions (A) depending on the initial concentration of NH_4^+ ions and (B) at the presence of competitive ions in real wastewater.

3.4.2. Presence of competitive ions

Samples of municipal wastewater were used in the CDI experiments to estimate the ammonium removal and recovery in the presence of competitive ions. The energy consumption required for the removal of target ions from the wastewater was also determined. Since the conventional wastewater treatment system is based on the activated sludge process, including the aerobic digestion focused on the removal of NH_4^+ ions via nitrification reactions, the wastewater

samples should be collected before the aeration. Thus, the primary clarifier was chosen as a sample point with the representative concentration of NH_4^+ ions (**Fig. S16**).

The electrosorption performance of the AC-ox electrode towards NH_4^+ ions in the presence of the competitive ions is illustrated in **Fig. 8 (C).** The specific time-dependent selectivity of the AC-ox electrode towards NH_4^+ ions was observed in a multicomponent solution. The time needed for the electrosorption of NH_4^+ ions decreased from 480 s (in the mono-component system) to 360 s (in the multi-component system) while the time required for the electrosorption of the other competitive ions was found to be 600 s. The monovalent NH_4^+ ions were electrosorbed firstly due to their higher initial concentration in the wastewater and the smallest hydrated radius providing the rapid diffusion towards the pores of the electrode material [56]. Additionally, the time-depended selectivity of the AC-ox electrode towards NH_4^+ ions could be a consequence of the surface complexation by oxygen-containing functional groups. On the other hand, the recovery of divalent ions (Ca^{2+} and Mg^{2+}) occurred at 720 s while the monovalent ions were discharged lastly at 840 s.

The maximum electrosorption capacity of 0.122 mmol/g of NH_4^+ ions was observed for the AC-ox electrode while the electrosorption capacity for Na^+, K^+, Ca^{2+} and Mg^{2+} ions were calculated to be 0.068, 0.035, 0.023, 0.008 mmol/g, respectively **(Fig. 9 (B))**. However, the highest removal efficiency of 29% was obtained for the case of K^+ ions almost as high as NH_4^+ removal of 25%. This could be because of the same hydration radius (3.31 Å) of NH_4^+ and K^+ ions. The removal efficiencies of Na^+, $Ca^{2+,}$ and Mg^{2+} ions were calculated to be 18%, 17%, and 14%, respectively. It should be noted here that Na^+, $Ca^{2+,}$ and Mg^{2+} ions have larger hydrated radii of 3.58, 4.12, and 4.28 Å, respectively, in comparison to NH_4^+ and K^+ ions. Hence, it is evident from these findings that the hydrated radius plays a governing role in influencing the ion removal

efficiency of the electrode. Likewise, the calculated selectivity coefficients (0.91 for NH_4^+/ K^+, 1.80 for NH_4^+/ Na^+, 1.95 for NH_4^+/ Ca^{2+}, and 2.35 for NH_4^+/ Mg^{2+}) indicated the higher selectivity separation of NH_4^+ over divalent ions with higher hydrated radii, induced by the stronger EDL overlapping effect [3].

The recovery efficiency of 2-5% was observed for all the ions in the first operating cycle which further increased to 4-10% during the second operational cycle. The desorption capacities were calculated to be 0.009 mmol NH_4^+/g, 0.004 mmol K^+ /g, 0.008 mmol Na^+ /g, 0.001 mmol Ca^{2+}/g, and 0.005 mmol Mg^{2+}/g. The ion recovery process was hindered, probably, due to the complex composition and high ionic strength of the feed solution, and the possible irreversible reactions on the surface of the carbon electrodes [56]. As activated carbon electrodes have a complex pore structure, not all of the ions can be released from the porous electrodes during the discharging stage [57]. Therefore, some ions remain in the pores of electrodes resulting in electrode saturation. Such aged electrodes cannot utilize the applied potential difference in full. Thus the electrostatic driving forces, responsible for the transport of the ions from the bulk solution into the electrodes and vice versa, are declined, and the CDI performance decreases [66].

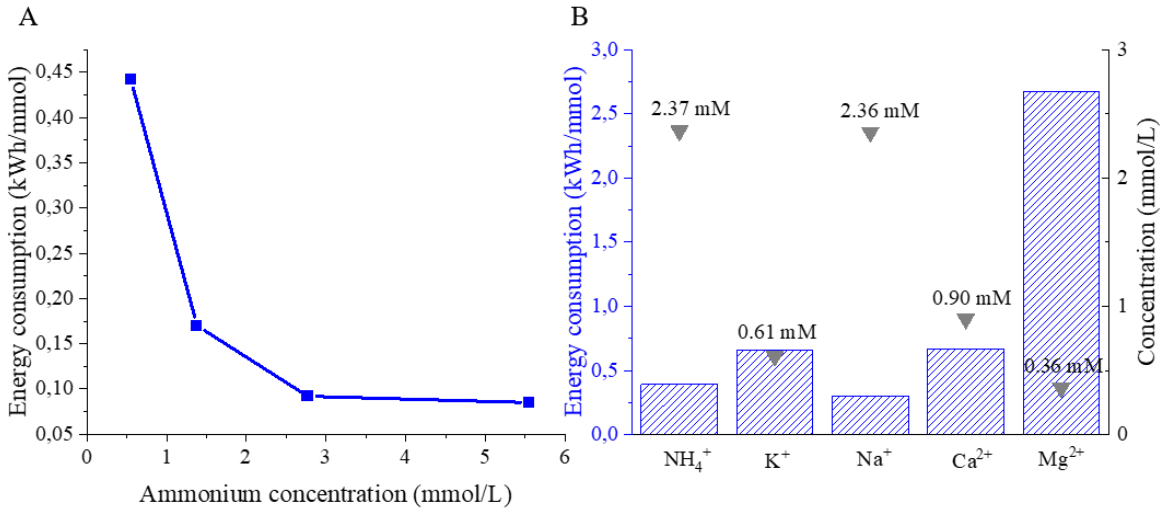

Fig. 10. Energy consumption A) depending on the initial concentration of the solution, B) required to remove ions from municipal wastewater.

The instantaneous current measured in the asymmetric CDI cell operated with municipal wastewater was about 60 mA **(Fig. 8 (D)**) while the transient current under the applied constant voltage of 1.2 V was maintained at 18 mA. The energy consumed for the removal of NH_4^+, K^+, Na+, Ca^{2+}, and Mg^{2+} ions from municipal wastewater was calculated to be 0.39, 0.66, 0.30, 0.67, and 2.67 kWh/mmol, respectively. The higher energy consumption was noted when the target ions are present in lower concentrations i.e. diluted streams (**Fig. 10 (B)**).

To sum up, the main results of this study were compared with the results recently reported in the literature and summarized in **Table 2**. Apparently, that oxygen functionalized AC electrode is competitive and even surpasses analogous systems in the removal efficiency and the electrosorption capacity.

Table 2. Comparison of the electrosorption capacities, removal, and recovery efficiencies among various carbon-based electrodes.

Electrode type	Tested solution	Mode	E, V	C_0 (NH_4^+), mg/L	η, %		R, %		Q, mg/g	Ref.
					Single	Multi	Single	Multi		
AC	Synthetic WW	SP	1.2	100	30	-	9	-	4.3.	This study
	Synthetic WW				83	-	20	-	12.1	
AC-ox	Municipal WW			43	-	25	-	5	2.2.	
AC (CDI) (MCDI) (fcMCDI)	Synthetic WW	BM	1	100	-	-	-	-	1.38 5.2 6.6	[67]
AC/Ni	Synthetic WW	-	1	50	55	-	-	-	6	[68]
CuHCF (MCDI)	Synthetic WW	-	0.3	180 - 1800	-	50	-	-	8.4	[69]
AC (fcMCDI)	Digestate WW	BM	1	865	-	54.4	-	-	4.5	[3]
AC cloth	Synthetic WW	BM	1.2	18	61	-	81.7	-	-	[20]
Graphene-based (MCDI)	Synthetic WW	BM	2	400	99	-	-	-	15.3	[70]
Graphene-based (CDI)	Synthetic WW	BM	2	18	36	-	77	-	8.4	[21]
					-	16	-	-	3.96	
AC (FCDI)	Synthetic WW	BM	1.2	20	87	73.5	82	-	1.21	[22]

WW - wastewater, SP – single-pass operating mode, BM – batch-mode, E – applied voltage, U – flow rate, C_0 - initial concentration, η - removal efficiency, R – recovery efficiency, Single - single-component system, Multi - multi-component system, Q - electrosorption capacity, MCDI – membrane CDI. FCDI – flow-electrode CDI.

Nonetheless, a lot of studies on ammonium removal and recovery by CDI and analogs have been conducted, the selective capability of CDI technology is still an open question and requires improvement and further development. For instance, intercalation electrodes or MOFs (metal-organic-frameworks) cover could contribute to the enhancing of the selectivity. Particular attention should be devoted to porous electrode fabrication as the main part of CDI units. Recently emerging technologies as additive manufacturing (AM) might be a promising solution for the production of mechanically stable materials with the customized structure. Additionally, the CDI process could be considered in a combination with pre-or-posttreatment technologies to achieve the highest removal and recovery efficiencies with acceptable energy consumption.

4. Conclusion

The application of CDI for the removal and recovery of NH_4^+ ions from municipal wastewater was investigated in this study. Material characterization, performed on AC before and after modifications, exhibited a reduction in the surface area of the materials, caused by the use of the polymeric binder and oxidation. Nonetheless, the enhanced wettability and added oxygen functionalities contribute to higher charge efficiency and the specific capacitance of the AC-ox electrode.

The symmetric and asymmetric CDI cell configurations were tested to estimate the electrosorption performance and the energy consumption during the CDI operation. Asymmetric CDI cell, equipped with the AC-ox cathode, demonstrated better electrosorption performance and lower energy consumption of 0.085 kWh/mmol NH_4^+, whereas the energy consumption by the

symmetric CDI cell was calculated to be 0.215 kWh/mmol NH_4^+. The enhanced CDI performance of the asymmetric cell is associated with well-balanced current distribution between the electrode pair due to the difference of the initial surface charges of the materials. The fabricated AC-ox electrode also demonstrated the higher removal efficiency of 83% and the highest electrosorption capacity of 0.67 mmol/g in comparison to the other reported values in the literature for NH_4^+ ion removal using the CDI process. The removal efficiency and the electrosorption capacity of the pristine AC electrode for NH_4^+ ions were only about 30% and 0.24 mmol/g, respectively. The recovery efficiency (20%) and the desorption capacity (0.32 mmol/g) of NH_4^+ ions by the AC-ox electrode were two-fold higher in comparison to the pristine AC electrode. Complex sorption mechanisms including the initial electrostatic attraction of ions by the oppositely charged electrodes, availability of the hydrophilic surface, formation of chemical bonds between oxygen functionalities and ammonium ions, and possible redox reactions are suggested for the description of the presented electrosorption process.

The efficiency of the electrosorption performance of the asymmetric CDI cell with municipal wastewater was lower because of the complex composition of wastewater and the presence of competitive ions. Nevertheless, the AC-ox electrode demonstrated the time-dependent selectivity and the highest electrosorption capacity of 0.122 mmol/g towards NH_4^+ ions in the multi-component system. The regeneration of the CDI electrodes under real municipal wastewater operation was found challenging because of the higher ionic strength of the feed solution. In conclusion, based on the observed results, we suggest the preferable electrosorption of NH_4^+ ions by the AC-ox electrode, the performance of which is governed mostly by the initial concentration of the ions in the feed solution and their hydration radius.

Acknowledgments

Financial support of this work from the European Regional Development Fund 2014-2020 (project code A73221) is gratefully appreciated. We would also like to acknowledge Kenkäveronniemi WWTP for the sampling support.

References

[1] H. Charles, H. Godfray, T. Garnett, Food security and sustainable intensification, Philos. Trans. R. Soc. B Biol. Sci. (2014). doi:10.1098/rstb.2012.0273.

[2] M. Shi, Z. Wang, Z. Zheng, E ff ect of Na + impregnated activated carbon on the adsorption of NH + 4 -N from aqueous solution, J. Environ. Sci. 25 (2013) 1501–1510. doi:10.1016/S1001-0742(8)60227-7.

[3] H. Sakar, I. Celik, C. Balcik-Canbolat, B. Keskinler, A. Karagunduz, Ammonium removal and recovery from real digestate wastewater by a modified operational method of membrane capacitive deionization unit, J. Clean. Prod. 215 (2019) 1415–1423. doi:10.1016/j.jclepro.2019.01.165.

[4] D.J. Batstone, T. Hülsen, C.M. Mehta, J. Keller, Platforms for energy and nutrient recovery from domestic wastewater: A review, Chemosphere. 140 (2015) 2–11. doi:10.1016/j.chemosphere.2014.10.021.

[5] B.E.R. Wen-Wei Li, Han-Qing Yu, Reuse water pollutants, Nature. 528 (2015) 3–5.

[6] Z. Wang, H. Gong, Y. Zhang, P. Liang, K. Wang, Nitrogen recovery from low-strength wastewater by combined membrane capacitive deionization (MCDI) and ion exchange (IE) process, Chem. Eng. J. 316 (2017) 1–6. doi:10.1016/j.cej.2017.01.082.

[7] D.I. Kim, P. Dorji, G. Gwak, S. Phuntsho, S. Hong, H. Shon, Reuse of municipal wastewater via membrane capacitive deionization using ion-selective polymer-coated carbon electrodes in pilot-scale, Chem. Eng. J. 372 (2019) 241–250. doi:10.1016/J.CEJ.2019.04.156.

[8] J. Yuan, Y. Ma, F. Yu, Y. Sun, X. Dai, J. Ma, Simultaneous in situ nutrient recovery and sustainable wastewater purification based on metal anion- and cation-targeted selective adsorbents, J. Hazard. Mater. 382 (2020) 121039. doi:10.1016/j.jhazmat.2019.121039.

[9] J.P. van der Hoek, R. Duijff, O. Reinstra, Nitrogen recovery from wastewater: Possibilities, competition with other resources, and adaptation pathways, Sustain. 10 (2018). doi:10.3390/su10124605.

[10] T. Zhang, X. Wu, S.M. Shaheen, Q. Zhao, X. Liu, J. Rinklebe, H. Ren, Ammonium nitrogen recovery from digestate by hydrothermal pretreatment followed by activated hydrochar sorption, Chem. Eng. J. 379 (2020). doi:10.1016/j.cej.2019.122254.

[11] J. Huang, N.R. Kankanamge, C. Chow, D.T. Welsh, T. Li, P.R. Teasdale, Removing ammonium from water and wastewater using cost-effective adsorbents: A review, J. Environ. Sci. (China). 63 (2018) 174–197. doi:10.1016/j.jes.2017.09.009.

[12] D.P. Smith, N.T. Smith, Local-scale recovery of wastewater nitrogen for edible plant growth, (2016) 1287–1292. doi:10.2166/wst.2015.598.

[13] D. Guaya, C. Valderrama, A. Farran, T. Sauras, J.L. Cortina, Valorisation of N and P from waste water by using natural reactive hybrid sorbents: Nutrients (N,P,K) release evaluation in amended soils by dynamic experiments, Sci. Total Environ. (2018). doi:10.1016/j.scitotenv.2017.08.248.

[14] H. Cruz, B. Laycock, E. Strounina, T. Seviour, A. Oehmen, I. Pikaar, Modified Poly(acrylic acid)-Based Hydrogels for Enhanced Mainstream Removal of Ammonium from Domestic Wastewater, Environ. Sci. Technol. 54 (2020) 9573–9583. doi:10.1021/acs.est.9b07032.

[15] S. Porada, R. Zhao, A. Van Der Wal, V. Presser, P.M. Biesheuvel, Review on the science and technology of water desalination by capacitive deionization, Prog. Mater. Sci. 58 (2013) 1388–1442. doi:10.1016/j.pmatsci.2013.03.005.

[16] S.A. Hawks, A. Ramachandran, S. Porada, P.G. Campbell, M.E. Suss, P.M. Biesheuvel, J.G. Santiago, M. Stadermann, Performance metrics for the objective assessment of capacitive deionization systems, Water Res. 152 (2019) 126–137. doi:10.1016/j.watres.2018.10.074.

[17] Z. Huang, L. Lu, Z. Cai, Z.J. Ren, Individual and competitive removal of heavy metals using capacitive deionization, J. Hazard. Mater. 302 (2016) 323–331. doi:10.1016/j.jhazmat.2015.09.064.

[18] S.J. Seo, H. Jeon, J.K. Lee, G.Y. Kim, D. Park, H. Nojima, J. Lee, S.H. Moon, Investigation on removal of hardness ions by capacitive deionization (CDI) for water softening applications, Water Res. 44 (2010) 2267–2275. doi:10.1016/j.watres.2009.10.020.

[19] L. Gan, Y. Wu, H. Song, S. Zhang, C. Lu, S. Yang, Z. Wang, B. Jiang, C. Wang, A. Li, Selective removal of nitrate ion using a novel activated carbon composite carbon electrode in capacitive deionization, Sep. Purif. Technol. 212 (2019) 728–736. doi:10.1016/j.seppur.2018.11.081.

[20] Z. Ge, X. Chen, X. Huang, Z.J. Ren, Capacitive deionization for nutrient recovery from wastewater with disinfection capability, Environ. Sci. Water Res. Technol. 4 (2018) 33–39. doi:10.1039/c7ew00350a.

[21] B. Xu, X. Xu, H. Gao, F. He, Y. Zhu, L. Qian, W. Han, Y. Zhang, W. Wei, Electro-enhanced adsorption of ammonium ions by effective graphene-based electrode in capacitive deionization, Sep. Purif. Technol. 250 (2020) 117243. doi:10.1016/j.seppur.2020.117243.

[22] K. Fang, H. Gong, W. He, F. Peng, C. He, K. Wang, Recovering ammonia from municipal wastewater by flow-electrode capacitive deionization, Chem. Eng. J. 348 (2018) 301–309. doi:10.1016/j.cej.2018.04.128.

[23] C. Zhang, J. Ma, D. He, T.D. Waite, Capacitive Membrane Stripping for Ammonia Recovery (CapAmm) from Dilute Wastewaters, Environ. Sci. Technol. Lett. 5 (2018) 43–49. doi:10.1021/acs.estlett.7b00534.

[24] C. Zhang, J. Ma, T.D. Waite, Ammonia-Rich Solution Production from Wastewaters Using Chemical-Free Flow-Electrode Capacitive Deionization, ACS Sustain. Chem. Eng. 7 (2019) 6480–6485. doi:10.1021/acssuschemeng.9b00314.

[25] B. Jia, W. Zhang, Preparation and Application of Electrodes in Capacitive Deionization (CDI): a State-of-Art Review, Nanoscale Res. Lett. 11 (2016) 1–25. doi:10.1186/s11671-016-1284-1.

[26] W. Yang, Y. Li, Y. Feng, High Electrochemical Performance from Oxygen Functional Groups Containing Porous Activated Carbon Electrode of Supercapacitors, Materials (Basel). 11 (2018) 1–10. doi:10.3390/ma11122455.

[27] M. Genovese, J. Jiang, K. Lian, N. Holm, High capacitive performance of exfoliated biochar nanosheets from biomass waste corn cob, J. Mater. Chem. A. 3 (2015) 2903–2913. doi:10.1039/c4ta06110a.

[28] K.-H. Park, C.-H. Lee, S.-K. Ryu, X. Yang, Zeta-potentials of Oxygen and Nitrogen Enriched Activated Carbons for Removal of Copper Ion, Carbon Lett. 8 (2007) 321–325. doi:10.5714/cl.2007.8.4.321.

[29] A. Rehman, M. Park, S.J. Park, Current progress on the surface chemical modification of carbonaceous materials, Coatings. 9 (2019) 1–22. doi:10.3390/COATINGS9020103.

[30] M.D. Stoller, R.S. Ruoff, Best practice methods for determining an electrode material's performance for ultracapacitors, Energy Environ. Sci. 3 (2010) 1294–1301. doi:10.1039/c0ee00074d.

[31] O. Pastushok, F. Zhao, D.L. Ramasamy, M. Sillanpää, Nitrate removal and recovery by capacitive deionization (CDI), Chem. Eng. J. (2019) 121943. doi:10.1016/j.cej.2019.121943.

[32] A.S. Yasin, M. Obaid, I.M.A. Mohamed, A. Yousef, N.A.M. Barakat, ZrO2nanofibers/activated carbon composite as a novel and effective electrode material for the enhancement of capacitive deionization performance, RSC Adv. 7 (2017) 4616–4626. doi:10.1039/c6ra26039j.

[33] S.A. Hawks, M.R. Cerón, D.I. Oyarzun, T.A. Pham, C. Zhan, C.K. Loeb, D. Mew, A. Deinhart, B.C. Wood, J.G. Santiago, M. Stadermann, P.G. Campbell, Using Ultramicroporous Carbon for the Selective Removal of Nitrate with Capacitive Deionization, Environ. Sci. Technol. 53 (2019) 10863–10870.

doi:10.1021/acs.est.9b01374.

[34] J. Lee, K. Jo, J. Lee, S.P. Hong, S. Kim, J. Yoon, Rocking-Chair Capacitive Deionization for Continuous Brackish Water Desalination, ACS Sustain. Chem. Eng. 6 (2018) 10815–10822. doi:10.1021/acssuschemeng.8b02123.

[35] M. Thommes, K. Kaneko, A. V. Neimark, J.P. Olivier, F. Rodriguez-Reinoso, J. Rouquerol, K.S.W. Sing, Physisorption of gases, with special reference to the evaluation of surface area and pore size distribution (IUPAC Technical Report), Pure Appl. Chem. 87 (2015). doi:10.1515/pac-2014-1117.

[36] K.S.W. Sing, R.T. Williams, Physisorption hysteresis loops and the characterization of nanoporous materials, Adsorpt. Sci. Technol. 22 (2004) 773–782. doi:10.1260/0263617053499032.

[37] M.M. Maroto-Valer, I. Dranca, T. Lupascu, R. Nastas, Effect of adsorbate polarity on thermodesorption profiles from oxidized and metal-impregnated activated carbons, Carbon N. Y. (2004). doi:10.1016/j.carbon.2004.06.007.

[38] Q. Abbas, D. Pajak, E. Frąckowiak, F. Béguin, Effect of binder on the performance of carbon/carbon symmetric capacitors in salt aqueous electrolyte, Electrochim. Acta. 140 (2014) 132–138. doi:10.1016/j.electacta.2014.04.096.

[39] D.L. Ramasamy, V. Puhakka, E. Repo, S. Ben Hammouda, M. Sillanpää, Two-stage selective recovery process of scandium from the group of rare earth elements in aqueous systems using activated carbon and silica composites: Dual applications by tailoring the ligand grafting approach, Chem. Eng. J. 341 (2018) 351–360. doi:10.1016/j.cej.2018.02.024.

[40] H. Liu, X. Wang, G. Zhai, J. Zhang, C. Zhang, N. Bao, C. Cheng, Preparation of activated carbon from lotus stalks with the mixture of phosphoric acid and pentaerythritol impregnation and its application for Ni(II) sorption, Chem. Eng. J. 209 (2012) 155–162. doi:10.1016/j.cej.2012.07.132.

[41] M. Genovese, J. Jiang, K. Lian, N. Holm, High capacitive performance of exfoliated biochar nanosheets from biomass waste corn cob, J. Mater. Chem. A. (2015). doi:10.1039/c4ta06110a.

[42] M.S. Islam, B.C. Ang, S. Gharehkhani, A.B.M. Afifi, Adsorption capability of activated carbon synthesized from coconut shell, Carbon Lett. 20 (2016) 1–9. doi:10.5714/CL.2016.20.001.

[43] T. Zheng, Q. Wang, Z. Shi, Z. Zhang, Y. Ma, Microwave regeneration of spent activated carbon for the treatment of ester-containing wastewater, RSC Adv. 6 (2016) 60815–60825. doi:10.1039/c6ra05211h.

[44] R. Ma, Y. Ma, Y. Gao, J. Cao, Preparation of micro-mesoporous carbon from seawater-impregnated sawdust by low temperature one-step CO2 activation for adsorption of oxytetracycline, SN Appl. Sci. 2 (2020). doi:10.1007/s42452-020-1940-z.

[45] G.N.G. Nifas, R.S. Forteza, Synthesis of Activated Carbon / Chitosan Composites and Expanded Graphite for Symmetric Supercapacitor Journal of Material Sciences & Engineering, 8 (2019).

[46] G. Zhang, L. Shi, Y. Zhang, D. Wei, T. Yan, Q. Wei, B. Du, Aerobic granular sludge-derived activated carbon: Mineral acid modification and superior dye adsorption capacity, RSC Adv. 5 (2015) 25279–25286. doi:10.1039/c4ra15216f.

[47] A. Rehman, M. Park, S. Park, Current Progress on the Surface Chemical Modification of Carbonaceous Materials, Coatings. (2019) 1–22. doi:10.3390/coatings9020103.

[48] G. Lu, G. Wang, P.H. Wang, Z. Yang, H. Yan, W. Ni, L. Zhang, Y.M. Yan, Enhanced capacitive deionization performance with carbon electrodes prepared with a modified evaporation casting method, Desalination. 386 (2016) 32–38. doi:10.1016/j.desal.2016.02.008.

[49] E. Frackowiak, F. Béguin, Carbon materials for the electrochemical storage of energy in capacitors, Carbon N. Y. 39 (2001) 937–950. doi:10.1016/S0008-6223(00)00183-4.

[50] N. Holubowitch, A. Omosebi, X. Gao, J. Landon, K. Liu, Quasi-Steady-State Polarization Reveals the Interplay of Capacitive and Faradaic Processes in Capacitive Deionization, ChemElectroChem. 4 (2017) 2404–2413. doi:10.1002/celc.201700082.

[51] C. Ma, J. Xu, Q. Fan, J. Shi, Y. Song, Synthesis and electrochemical performance of high surface area hierarchical porous carbon with ultrahigh mesoporosity for high-performance supercapacitors, J. Solid State Electrochem. 23 (2019) 2153–2163. doi:10.1007/s10008-019-04316-3.

[52] G. Folaranmi, M. Bechelany, P. Sistat, M. Cretin, F. Zaviska, Comparative investigation of activated carbon electrode and a novel activated carbon/graphene oxide composite electrode for an enhanced capacitive deionization, Materials (Basel). 13 (2020) 1–14. doi:10.3390/ma13225185.

[53] P.M. Biesheuvel, J.E. Dykstra, Physics of Electrochemical Processes, 2020. http://www.physicsofelectrochemicalprocesses.com.

[54] J. Lee, P. Srimuk, S. Fleischmann, X. Su, T.A. Hatton, V. Presser, Redox-electrolytes for non-flow electrochemical energy storage: A critical review and best practice, Prog. Mater. Sci. 101 (2019) 46–89. doi:10.1016/j.pmatsci.2018.10.005.

[55] V. Khomenko, E. Frackowiak, F. Béguin, Determination of the specific capacitance of conducting polymer/nanotubes composite electrodes using different cell configurations, Electrochim. Acta. 50 (2005) 2499–2506. doi:10.1016/j.electacta.2004.10.078.

[56] D.I. Kim, P. Dorji, G. Gwak, S. Phuntsho, S. Hong, H. Shon, Effect of Brine Water on Discharge of Cations in Membrane Capacitive Deionization and Its Implications on Nitrogen Recovery from Wastewater, ACS Sustain. Chem. Eng. 7 (2019) 11474–11484. doi:10.1021/acssuschemeng.9b01286.

[57] I. Cohen, E. Avraham, Y. Bouhadana, A. Soffer, D. Aurbach, Long term stability of capacitive de-ionization processes for water desalination: The challenge of positive electrodes corrosion, Electrochim. Acta. 106 (2013) 91–100. doi:10.1016/j.electacta.2013.05.029.

[58] C. Santos, J.J. Lado, E. García-Quismondo, J. Soria, J. Palma, M.A. Anderson, Maximizing Volumetric Removal Capacity in Capacitive Deionization by Adjusting Electrode Thickness and Charging Mode, J. Electrochem. Soc. 165 (2018) E294–E302. doi:10.1149/2.1011807jes.

[59] M. Metzger, M.M. Besli, S. Kuppan, S. Hellstrom, S. Kim, E. Sebti, C. V. Subban, J. Christensen, Techno-economic analysis of capacitive and intercalative water deionization, Energy Environ. Sci. 13 (2020) 1544–1560. doi:10.1039/d0ee00725k.

[60] H. Li, L. Pan, C. Nie, Y. Liu, Z. Sun, Reduced graphene oxide and activated carbon

composites for capacitive deionization, J. Mater. Chem. 22 (2012) 15556–15561. doi:10.1039/c2jm32207b.

[61] S. Ntakirutimana, W. Tan, M.A. Anderson, Y. Wang, Editors ' Choice — Review — Activated Carbon Electrode Design : Engineering Tradeoff with Respect to Capacitive Deionization Performance Editors ' Choice — Review — Activated Carbon Electrode Design : Engineering Tradeoff with Respect to Capacitive Deioni, J. Electrochem. Soc. (2020). doi:10.1149/1945-7111/abbfd7.

[62] X. Xu, L. Pan, Y. Liu, T. Lu, Z. Sun, D.H.C. Chua, Facile synthesis of novel graphene sponge for high performance capacitive deionization, Sci. Rep. (2015). doi:10.1038/srep08458.

[63] T. Wu, G. Wang, Q. Dong, B. Qian, Y. Meng, J. Qiu, Asymmetric capacitive deionization utilizing nitric acid treated activated carbon fiber as the cathode, Electrochim. Acta. 176 (2015) 426–433. doi:10.1016/j.electacta.2015.07.037.

[64] J.J. Lado, R.E. Pérez-Roa, J.J. Wouters, M. Isabel Tejedor-Tejedor, M.A. Anderson, Evaluation of operational parameters for a capacitive deionization reactor employing asymmetric electrodes, Sep. Purif. Technol. 133 (2014) 236–245. doi:10.1016/j.seppur.2014.07.004.

[65] C. Zhang, D. He, J. Ma, W. Tang, T.D. Waite, Comparison of faradaic reactions in flow-through and flow-by capacitive deionization (CDI) systems, Electrochim. Acta. 299 (2019) 727–735. doi:10.1016/j.electacta.2019.01.058.

[66] S. Porada, M. Bryjak, A. Van Der Wal, P.M. Biesheuvel, Effect of electrode thickness variation on operation of capacitive deionization, Electrochim. Acta. 75 (2012) 148–156.

doi:10.1016/j.electacta.2012.04.083.

[67] H. Sakar, I. Celik, C. Balcik Canbolat, B. Keskinler, A. Karagunduz, Electro-sorption of ammonium by a modified membrane capacitive deionization unit, Sep. Sci. Technol. 52 (2017) 2591–2599. doi:10.1080/01496395.2017.1336556.

[68] Y.J. Shih, C. Di Dong, Y.H. Huang, C.P. Huang, Loofah-derived activated carbon supported on nickel foam (AC/Ni) electrodes for the electro-sorption of ammonium ion from aqueous solutions, Chemosphere. 242 (2020) 125259. doi:10.1016/j.chemosphere.2019.125259.

[69] M. Son, B.L. Aronson, W. Yang, C.A. Gorski, B.E. Logan, Recovery of ammonium and phosphate using battery deionization in a background electrolyte, Environ. Sci. Water Res. Technol. 6 (2020) 1688–1696. doi:10.1039/d0ew00183j.

[70] Y. Wimalasiri, M. Mossad, L. Zou, Thermodynamics and kinetics of adsorption of ammonium ions by graphene laminate electrodes in capacitive deionization, Desalination. 357 (2015) 178–188. doi:10.1016/j.desal.2014.11.015.